Chapter 9

Physical Properties of Porous Pure and Zr/Sn-Doped Nanocrystalline $BaTiO_3$ Ceramics

Umaru Ahmadu, Alhassan Muazu and Sadiq Umar

Additional information is available at the end of the chapter

http://dx.doi.org/10.5772/intechopen.75500

Abstract

Polycrystalline $BaTiO_3$ and $Ba(Ti_{0.96}SnxZr_{0.04-x})O_3$ ceramics (x = 0.02-0.04) were prepared by a combination of solid-state and mechanochemical process and characterized at room temperature by X-ray diffraction for phase composition. Their crystal structures were found to be of the cubic and tetragonal symmetries, respectively. The grain size and porosity which were determined using Field Emission Scanning Electron Microscope (FESEM) and densitometer, respectively showed decrease and increase of relative density respectively, with increase in doping concentration. The variations of dielectric constant and loss with frequency and temperature show a maximum dielectric constant of 1660 at room temperature for $Ba(Ti_{0.96}Sn_{0.03}Zr_{0.01})O_3$. The remnant polarization (P_r) and coercive field (E_c) of BT were found to be 581.73 V/cm and 0.27 μC/cm^2. Increase in Sn content led to an increase in Pr of 0.58, 3.07, 3.73 C/cm^2, and Ec of 1766.8, 2855.7, 2661.1 V/cm, respectively and are expected to lead to a significant reduction in the thickness of the multilayer ceramic capacitors. Impedance spectroscopy of polycrystalline Ba $(Ti_{0.96}Sn_{0.02}Zr_{0.02})$ O_3 in a wide frequency and temperature range showed Nyquist plots with presence of grain and grain boundary at 400°C and a negative temperature coefficient of resistance (NTCR) for $Ba(Ti_{0.96}Sn_{0.02}Zr_{0.02})O_3$. The dielectric relaxation showed a non-Debye character.

Keywords: porous ceramics, barium titanate, doping, ferroelectrics, MLCC

1. Introduction

1.1. $BaTiO_3$ and $Ba(Ti_{0.96}Sn_xZr_{0.04-x})O_3$

Barium titanate (BT) is one of the most basic and widely applied ferroelectric oxide materials with a perovskite-ABO_3 type crystalline structure. It is chemically and mechanically remarkably stable and exhibits ferroelectric properties from room temperature to just below the transition

temperature (T_c). It is easily prepared and used in polycrystalline ceramic form [1]. Due to its excellent dielectric, ferroelectric, piezoelectric, pyroelectric and optoelectric properties, it is extensively used in multilayer ceramic capacitors (MLCC), positive temperature coefficient of resistance (PTCR) thermistors, piezoelectric sensors, actuators, ferroelectric random access memories (FRAM) and electro-optic devices [2, 3]. Pure BT is an electric insulator with a large energy gap of 3.05 eV at room temperature. However, when doped with small metals, it becomes semiconducting and leads to possibilities of tailoring its properties for specific technological applications. Modified BT compositions are widely used in MLCCs due to its high dielectric constant and low loss [4]. Among the doped BT compositions, $Ba(Ti_{1-x}Sn_x)O_3$ (BST) system has drawn wide attention due to its manifestation of diffuse-type phase transition [5–7] and many dielectric applications with reduction of phase transition temperature toward room temperature [8, 9]. Zirconium-doped barium titanate with general formula $Ba(Zr_xTi_{1-x})O_3$ (BZT) has attracted great attention for its potential applications due to its high dielectric constant, relatively low dielectric losses, large voltage tunability of the dielectric constant, as well as a good chemical stability [10–12]. Partial replacement of titanium by tin, zirconium or hafnium generally leads to a reduction in T_c and an increase in the permittivity maximum (ε_{max}) with increase in dopant content [13]. The substitution of isovalent cations Zr^{+4} and Sn^{+4} for Ti^{+4} lead to the formation of barium titanate stannate zirconate compound which belongs to the class of complex perovskite structure having the general formula $ABB''_xB''_{4-x}O_3$ (A,B, are the cation, $B''_xB''_{4-x}$ are the isovalent cation dopants and O_3 anion). These compounds have been widely studied owing to their very high and broad relative permittivity at the ferroelectric Curie point. Therefore, codoping of BT with two tetravalent ions Zr^{+4} and Sn^{+4} would be a good strategy to tailor the properties of porous BT ceramics.

There are challenges, however, one of which is in developing a dielectric layer of fewer than 10 μm with a large capacitance, a major requirement for MLCC miniaturization and electronic/microelectronic devices [14]. Reduction of the grain size of BT ceramics to the micron level leads to an increase in permittivity at room temperature. Further reduction of grain size to less than few hundred nanometers leads to a further decrease in permittivity. On the other hand, the presence of porosity can lead to dielectric permittivity that is lower than that of the solid material. It is thus one strategy to achieve lower dielectric constants for microelectronics devices. Thus, controlling porosity can yield a spectrum of dielectric constants from a single material [15]. Porosity plays a role in decreasing the Curie point for barium titanate ceramics with apparent density below 90% [16]. Manipulation of the volume ratio of porosity can lead to appropriate dielectric constant being obtained in a wide range. These advantages have been harnessed in the fabrication of materials with highly anisotropic dielectric constants with simultaneous introduction of aligned pores [17]. High material porosity is considered as an advantage only in few cases such as in materials that have resistance to temperature changes.

Various techniques have been introduced to make mesoporous and porous $BaTiO_3$ some of which include, development of soft-chemistry routes to produce nanoparticles or specially shaped materials, such as one-dimensional nanowires; sonochemical methods to prepare size-tunable $BaTiO_3$ crystals [18] and the introduction of biosynthesis methods to prepare $BaTiO_3$ nanopowders [19]. Mesoporous and porous materials have important features such as the

possession of large surface areas and nano size porous structures [20]. These features make the materials widely used in photo electronics, catalytic reactions and semiconductors among others [21, 22]. However, the high costs and difficulty in process control in these routes necessitated the development of alternative options for the synthesis of porous $BaTiO_3$ nanoparticles.

Mechanochemical synthesis can be used to reduce the grain size of porous $BaTiO_3$ and Ba $(Ti_{0.96}Sn_xZr_{0.04-x})$ O_3 (x = 0.02−0.04) powder to nanosize. This is predicated on the fact that mechanical technique is superior to both the conventional solid-state reaction and wet-chemistry-based processing routes for several reasons as it uses low-cost and widely available oxides as starting materials compared to wet chemical routes which are extremely sensitive to environmental conditions such as moisture, light and heat [23, 24].

Complex impedance spectroscopy is a nondestructive method [25] that uses to distinguish the grain boundary from the grain-electrode effects which are usually the sites for trapping oxygen vacancies and other defects. Within a wide range of ceramics, an ionic, ionic plus electronic or electronic conduction is shown in these sites. It is also useful in establishing space charge polarization and its relaxation mechanism, by appropriately attributing different values of resistance and capacitance to the grain and grain boundary effects. It allows the contributions to the overall electrical property by various components in the material to be easily separated. Other workers have used impedance spectroscopy to study other materials [26, 27] to gain insight into electrical conduction mechanisms of the materials. In this work, we report the structural and electrical properties of porous $BaTiO_3$ and $Ba(Ti_{0.96}Sn_xZr_{0.04-x})O_3$ (x = 0.02−0.04) ceramics prepared by solid-state and mechanochemical technique. The effect of porosity on the ceramics material will be used to evaluate the materials and serve as guide in the choice for MLCC and thermistor applications.

1.2. Mechanochemical synthesis

Mechanochemical synthesis or high-energy milling is the preparation of powder by high-energy ball milling of elemental mixtures. The most important feature of this technique is that the formation of the product compounds flows from the reactions of oxide precursors by mechanical energy activation, rather than the heat energy necessitated in the conventional solid-state reaction process.

The solid-state reactions initiated by intensive milling in high-energy ball mills could be a good choice for the ceramic powder preparation. The area of contact between the reactant powder particles increases with the intensive milling. This is the consequence of reduction in particle size and permits fresh surfaces to come into contact. This permits the reduction to continue without the requirement for diffusion through the product layer. Alternatively, the particle refinement and consequent reduction in diffusion distances (due to microstructural refinement) can at least reduce the reaction temperatures significantly, even if they do not occur at room temperature. In general, the procedure of sintering is improved by liquid-phase sintering with titanium-rich composition at the temperature above 1320°C or by mechanical activation of precursors ($BaCO_3$ and TiO_2) [28–30]. In addition, particle size of ceramic powders is reduced by mechanical

treatment and produces nanostructured powders which are of primary interest in the current trend of miniaturization and integration of electronic components [31, 32].

1.3. Barium titanate ($BaTiO_3$) perovskite structure

The perovskite, ABO_3 type structure of BT is cubic (above 120°C) with Ba ion (larger A cation) located at the cube corners, Ti ion (smaller B cation) at the body center, and oxygen at the face centre, forming octahedra around each Ti ion. It is considered an FCC-derivative structure in which the larger A cation and oxygen together form an FCC lattice, while the smaller B cation occupies the octahedral interstitial sites in the FCC array. The Ba ion occupies the space formed between eight neighboring octahedra, giving the Ba, Ti and the oxygen ions coordination number of 12, 6 and 6, respectively. $BaTiO_3$ can accept the substitution of foreign cations on two distinct sites, the A-site (Ba) and the B-site (Ti). The stability of the perovskite compounds arises mainly from the electrostatic charge of the ions when perfectly integrated.

1.4. Structural phase transitions in barium titanate

BT undergoes a series of structural phase transitions upon cooling from high temperature. In the temperature range of 1430–1620°C, barium titanate assumes a hexagonal structure. In the 130–1430°C range, BT is cubic and nonpolar (space group *Pm3m),* thus centrosymmetric and nonpiezoelectric. When the temperature is below the Curie temperature (130°C), the cubic structure (paraelectric) is slightly distorted to a tetragonal *(P4mm)* structure (ferroelectric) which is noncentrosymmetric, with an accompanying movement of Ti atoms inside the O_6 octahedra. In turn, oxygen ions all shift in the opposite direction [100]. Not only does this result in distortion of oxygen octahedron, but the opposite displacement of negative and positive charges within the unit cell leads to the formation of an electric dipole moment, and hence to the appearance of spontaneous polarization and ferroelectric properties. In the tetragonal phase, the direction of the vector of spontaneous polarization Ps (i.e., polar direction) lies parallel to the direction of one of the original cubic [100] directions. When the temperature is below 5°C, the tetragonal structure transforms to an orthorhombic ferroelectric phase *(C2mm)* with the polar axis parallel to a face diagonally, and the direction of spontaneous polarization transfers to a pseudocubic [110]. At as low as −90°C, it further transforms to a rhombohedral structure *(R3m)* with the polar axis along a body diagonal and is spontaneously polarized along a [111] direction.

The Goldschmidt tolerance factor for a perovskite structure (ABO_3) is given by the formula:

$$t = \frac{r_A + r_O}{\sqrt{2}(r_B + r_O)} \tag{1}$$

where r_A r_B and r_O are the A-site, B-site, and oxygen ionic radii, respectively. There are three possible values of '*t*': (1) $t \geq 1$: show ferroelectricity. (2) $t < 1$: This antiferroelectric perovskite. (3) $t = 1$: perfect cubic structure.

2. Experimental

2.1. Sample preparation

All samples used in this study were prepared by the conventional solid state and mechano-chemical technique from fine powders of metal oxides or metal carbonates. The nominal purity of the initial powders, as well as their manufacturers are given in **Table 1**.

2.2. Synthesis of barium titanate ($BaTiO_3$) and Zr- and Sn-doped barium titanate

$BaTiO_3$and $Ba(Ti_{0.96}Sn_xZr_{0.04-x})O_3$ (x = 0.02−0.04) nanocrystalline powders were synthesized by a combination of solid-state reaction and high-energy ball milling technique. The starting materials were analytical grade high-purity (99·9%) oxide precursors, $BaCO_3$, ZrO_2, TiO_2 and SnO_2. Stoichiometric amounts of the oxides were weighed according to nominal composition and ball-mixed for 12 h in alcohol. The mixture was dried in an oven and calcined in an alumina crucible at 1050°C for 4 h in the air to yield $BaTiO_3$, $Ba(Ti_{0.96}Sn_{0.02}Zr_{0.02})O_3$, $Ba(Ti_{0.96}Sn_{0.03}Zr_{0.01})O_3$, and $Ba(Ti_{0.96}Sn_{0.04})O_3$ powders. The calcined powders were ball-milled in an isopropyl alcohol as wetting medium using SPEX 8000 Mixer/Mills (60 Hz model) at room temperature for 7 h. The milling was stopped for 15 min after every 60 min of milling to cool down the system. The slurry was put in an oven and dried at 90°C for 24 h. The milled powder was compacted at 5 ton to make pellets of size 15 mm in diameter and 1.5 mm in thickness using polyvinyl alcohol (PVA) as a binder. After burning off the binder (PVA), the pellets were sintered in a programmable furnace at temperatures of 1190°C for 2 h in alumina crucibles.

2.3. Characterization

Phase identification of calcined and sintered powders was carried out using X-ray diffractometer with monochromatic Cu-Kα radiation (λ = 1.54178 Å) under 40 kV/30 mA—over a 2θ range from 20 to 80° at a scanning rate of 2°/min. The experimental densities of the samples were calculated using Electronic Densimeter MD-3005 ALFAMIRAGE. The morphological studies of the sintered sample were carried out using field-emission scanning electron microscopy (FE-SEM) (JEOL 7600F) operated at 15 kV. The polarization-electric field (P–E) hysteresis

Starting materials	Manufacturers	Purity
$BaCO_3$	Merck, Germany	99.9%
TiO_2	Aldrich Chemical Company, Inc.,U.S.A	99.9+%
SnO_2	Strem, Chemicals, U.S.A.	99.9%
ZrO_2	Strem, Chemicals, U.S.A	99.9%

Table 1. Precursors, purity level and manufacturers.

characteristics of the samples were determined using a Precision LC material analyzer (Radiant, U.S.A). The dielectric and impedance measurement was carried out for the sintered sample using an Agilent 4294 A Impedance Analyzer in the frequency and temperature range of 40 Hz–1 MHz and 30–400°C, respectively.

3. Structural and electrical properties

3.1. Structural properties

Structural and dielectric properties were evaluated for both $BaTiO_3$ and $Ba(Ti_{0.96}Sn_xZr_{0.04-x})O_3$ (x = 0.02−0.04) ceramic, while thermistor application is explored in Ba $(Ti_{0.96}Sn_{0.02}Zr_{0.02})O_3$ ceramic

3.1.1. XRD analysis

Figure 1 shows the room temperature XRD patterns of $BaTiO_3$ and $Ba(Ti_{0.96}Sn_xZr_{0.04-x})O_3$ (x = 0.02−0.04) ceramics. It is seen that all the compositions are of single-phase perovskite structure without any trace of secondary phase and imply that Sn^{+4} and Zr^{+4} entered the unit cell and maintained the perovskite structure as a solid solution. The enlarged XRD patterns of the ceramics in the range of $2\boldsymbol{\theta}$ of 44–46.5° clearly show that the crystal structure of the ceramic is cubic for BT with JCPDS file no. 96-150-7758 and space group *Pm-3 m* (**Figure 2a**). This is because the (200) and (002) peaks are not split [33] as reported by other workers [34, 35], whereas it is tetragonal for $Ba(Ti_{0.96}Sn_xZr_{0.04-x})O_3$ (x = 0.02−0.04) (**Figure 2b–d**) with the splitting of the (200) and (002) characteristic peaks which are in agreement with the **j**oint **c**ommittee on **p**owder **d**iffraction **s**tandards (JCPDS file no.98-00-2020), similar result was obtained for x = 0.04 using conventional method by other workers [36]. It can also be noticed from **Figure 2a–d** that the positions of the diffraction peaks of the ceramics shift slightly to lower angle with increasing Sn content in the range of $2\boldsymbol{\theta}$ from 44 to 46.5°. This is attributed to the larger ionic radius of Sn^{+4} (0.69 Å) and Zr^{+4} (0.72 Å) as compared with that of Ti^{+4} (0.60 Å) with results in a slight enlargement of crystal cell volumes and hence a shift of diffraction peaks toward lower angles.

3.1.2. Microstructure

Figures 3–6 show the FE-SEM images of porous $BaTiO_3$ and $Ba(Ti_{0.96}Sn_xZr_{0.04-x})O_3$ (x = 0.02−0.04) ceramic sintered at 1190°C for 2 h. All the samples are dense and have varying microstructural features with the presence of voids. The presence of voids in the FE-SEM images indicates that the pellets have a certain amount of porosity. The grain size and grain boundary can be seen very clearly in a nonagglomerated region and the grain size decreases with increasing Sn content. The difference among these four samples is attributed to the difference in Sn and Zr content since all of them have been processed under the same conditions. Further substitution of Sn caused the grain size to become smaller with more porous regions between them compared to porous $BaTiO_3$ sample. The average grain size of $BaTiO_3$ and $Ba(Ti_{0.96}Sn_xZr_{0.04-x})O_3$ (x = 0.02−0.04) ceramics determined by using linear intercept technique is shown in **Table 2**. The

http://dx.doi.org/10.5772/intechopen.75500

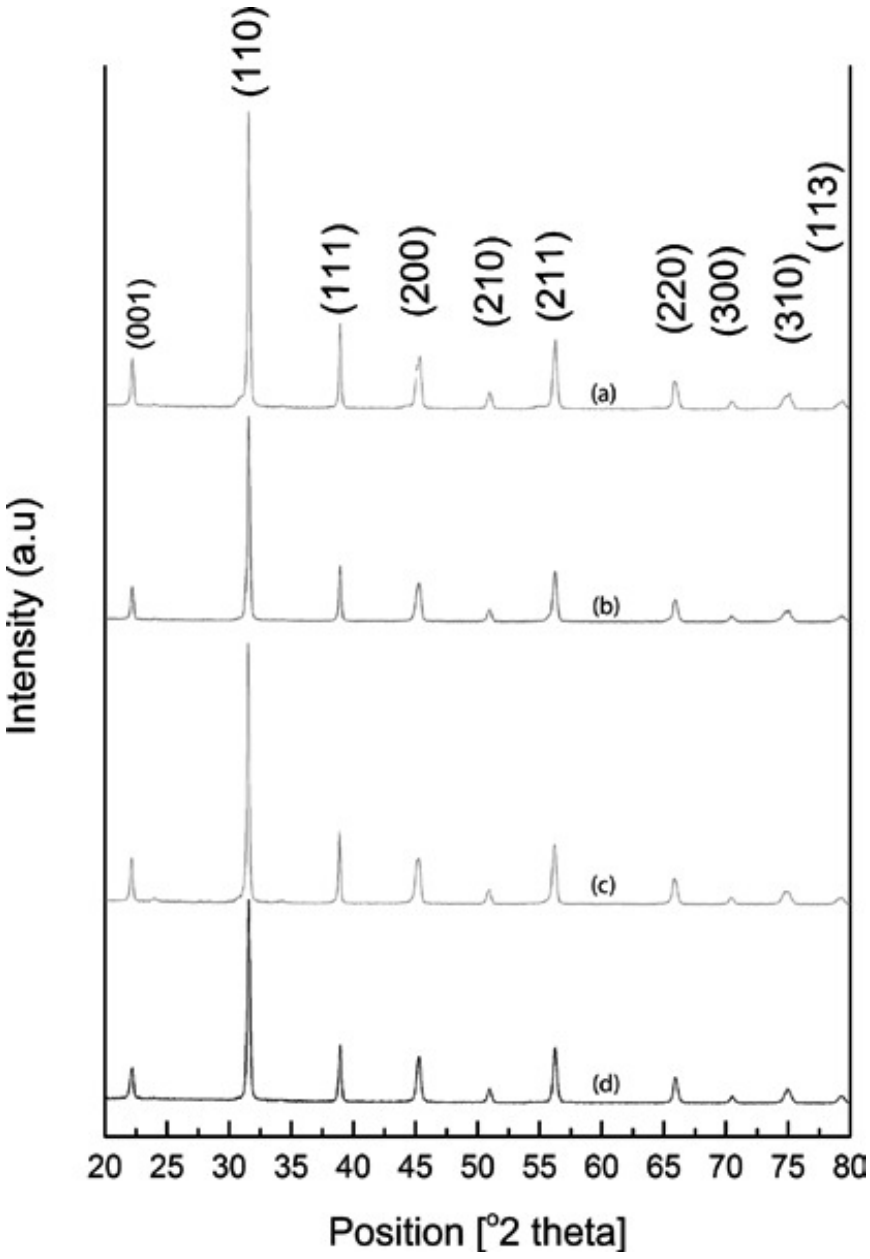

Figure 1. XRD patterns of $BaTiO_3$ and $Ba(Ti_{0.96}Sn_xZr_{0.04-x})O_3$ ceramics (a) BT, (b) 0.02, (c) 0.03 and (d) 0.04 sintered at 1190°C.

grain size decreased from 199.65 to 89.28 nm with increase in Sn and this indicates that Sn is a grain growth inhibitor.

3.1.3. Density

The experimental or observed density of each sample was calculated using the Archimedes principle from (Eq. (2)):

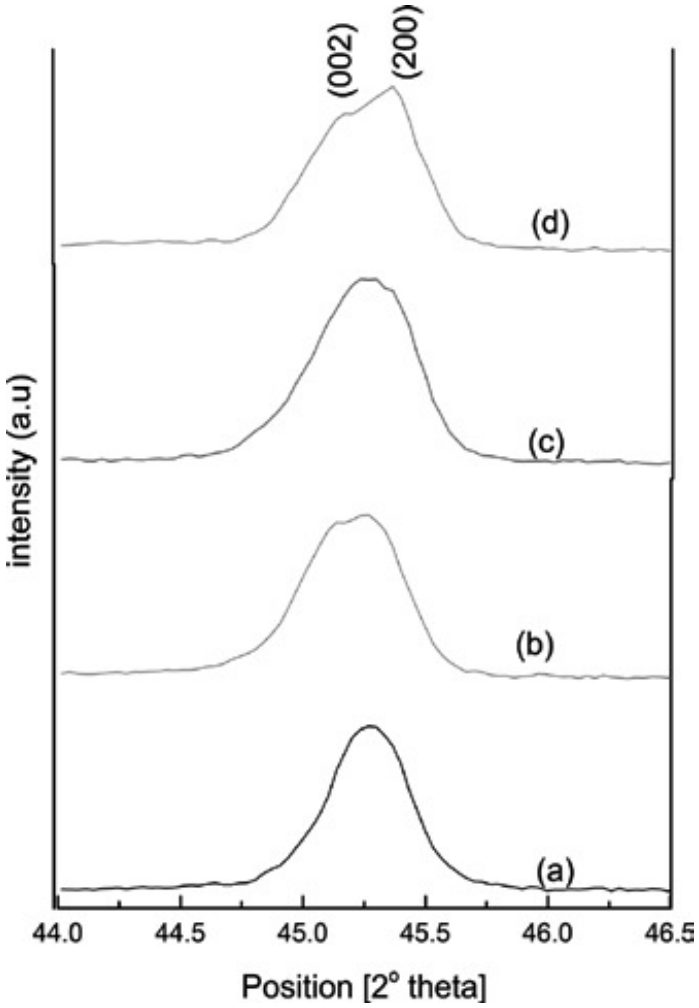

Figure 2. XRD patterns of $BaTiO_3$ and $Ba(Ti_{0.96}Sn_xZr_{0.04-x})O_3$ ceramics in the range of 2θ from 44 to 46.5° (a) BT, (b) 0.02, (c) 0.03 and (d) 0.04 sintered at 1190°C.

$$\boldsymbol{\rho}_{exp} = \frac{\boldsymbol{M_a \rho_w}}{\boldsymbol{M_a - M_w}} \tag{2}$$

where *Ma* and *Mw* are the respective weights in gram of the pellet measured in air and in water. $\rho_{w\ is}$ the density of pure water in g/cm^3. The theoretical density of the material was calculated using (Eq. (3)):

$$\boldsymbol{\rho_{xrd}} = \frac{\boldsymbol{cell\ mass}}{\boldsymbol{cell\ volume}} = \frac{\frac{n \times M \times 1.66 \times 10^{-24}}{V} g}{cm^3}, \tag{3}$$

where n is the number of atoms per unit cell, M is the molecular weight of atoms constituting one unit of the chemical formula, and V is the unit cell volume.

http://dx.doi.org/10.5772/intechopen.75500

The experimental densities of the porous $BaTiO_3$ and $Ba(Ti_{0.96}Sn_xZr_{0.04-x})O_3$ (x = 0.02−0.04) ceramics prepared by High Energy Mechanochemical (HEM) method and conventional sintering vary from 93.6% to 89.0%of theoretical density. The relative density of $BaTiO_3$ is higher compared to the Sn-/Zr-doped samples. The increase of the tin content to x = 0.04 induced further densification which tends to inhibit the grain growth [37]. This increase in density is also evident in FESEM microstructures of **Figures 3–6** which show a decreasing presence of porosity with increasing Sn content.

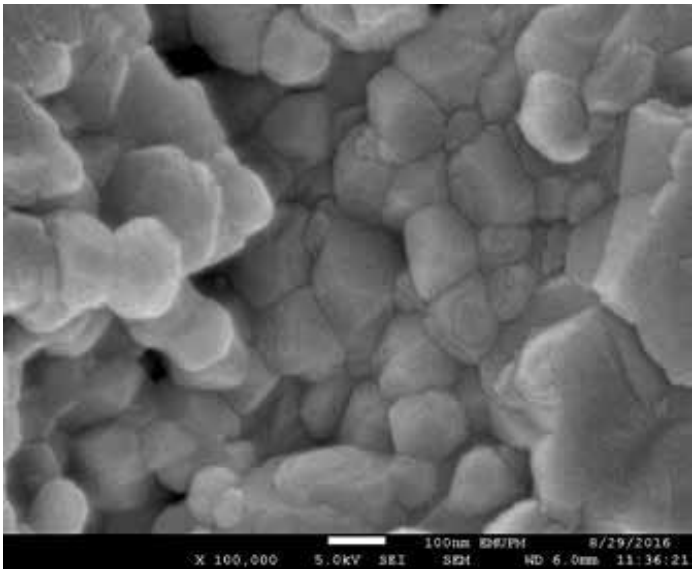

Figure 3. FESEM images of nanocrystalline BT sample at magnification of ×200,000.

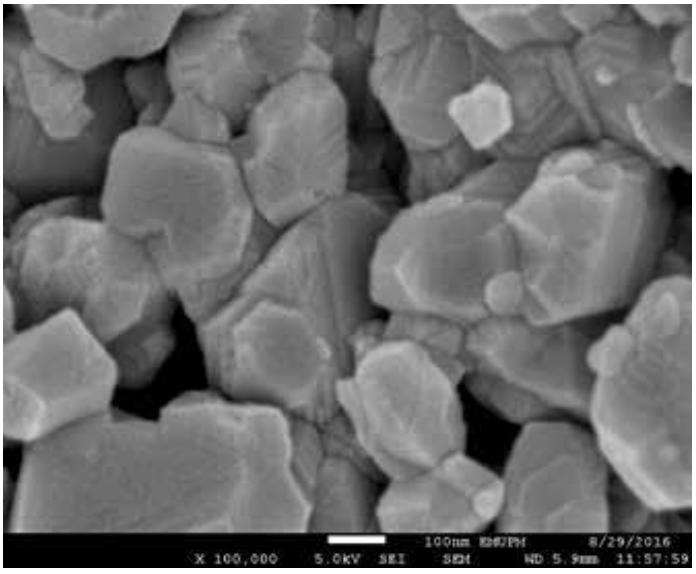

Figure 4. FESEM images of nanocrystalline $Ba(Ti_{0.96}Sn_xZr_{0.04-x})O_3$ (x = 0.02) sample at magnification of ×200,000.

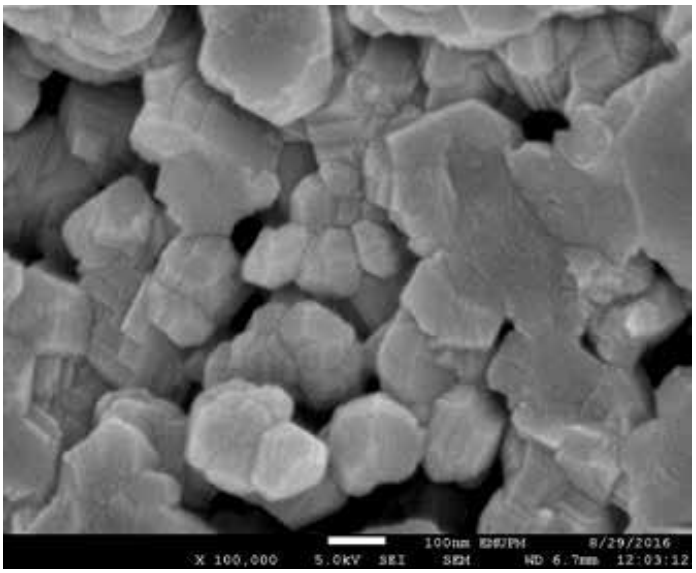

Figure 5. FESEM images of nanocrystalline $Ba(Ti_{0.96}Sn_xZr_{0.04-x})O_3$ (x = 0.03) sample at magnification of ×200,000.

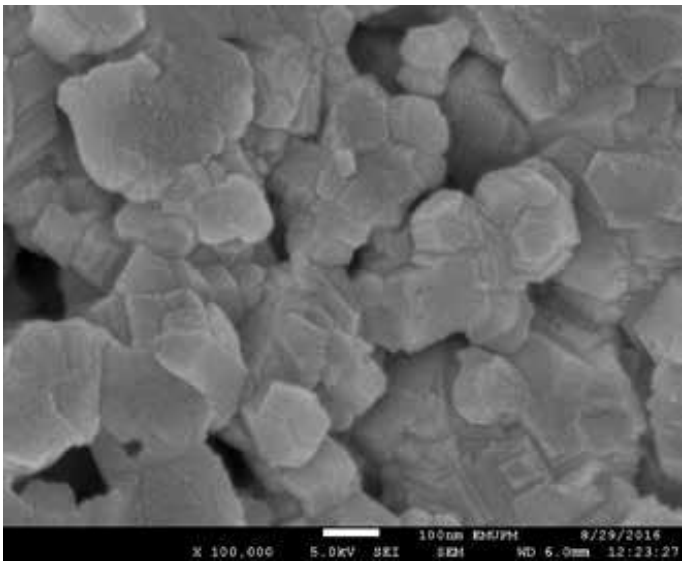

Figure 6. FESEM images of nanocrystalline $Ba(Ti_{0.96}Sn_xZr_{0.04-x})O_3$ (x = 0.04) sample at magnification of ×200,000.

3.1.4. Porosity

The porosity of $BaTiO_3$ and $Ba(Ti_{0.96}Sn_xZr_{0.04-x})O_3$ (x = 0.02−0.04) ceramics was calculated using (Eq. (4)):

$$\text{Porosity} = \left(d_{xrd} - d_{\exp}\right) \times \frac{100}{d_{xrd}} \tag{4}$$

The macroporous structure of $BaTiO_3$ and $Ba(Ti_{0.96}Sn_xZr_{0.04-x})O_3$ (x = 0.02−0.04) ceramics exhibited a porosity of 6.3–10.9% **Table 2**. Porosity increased from 6.3 to 12.8% at $Ba(Ti_{0.96}Sn_{0.02}Zr_{0.02})O_3$ and then decreased to 10.9% with increase in Sn concentration, respectively. The increase of the relative density and decrease of porosity with Sn concentration enhance the density of the ceramics with reduction of pores. It can be seen from the FESEM image in **Figures 3–6** that the pores vary in sizes in all the samples. Pores are composed of macropores in the grain boundary or nanopores in the grains, but in all the samples, only macropores are visible.

3.1.5. Effect of porosity on dielectric properties

Porosity in BT ceramics can be considered as a secondary phase and indicates its degree of densification. Pores in BT ceramics are usually formed by incomplete sintering or using sacrificial pore formers and exist in between the grains. Porosity decreases strength, because pores reduce the true cross section area of a BT ceramics and also pores act as stress concentrating notches. In many cases, different densities within a ceramic are used to provide a wide continuous range of dielectric constants. The relative permittivity decreases with increasing material porosity as reported by other workers [38]. Porosity of a ceramic material is a serious defect in high-voltage insulating systems [39]. Enhanced electric field in the pores increases the probability of bond breakage on the pore walls and leads to the lowering of the overall breakdown strength [40].

3.2. Dielectric properties

3.2.1. Variation of dielectric constant and loss tangent with frequency

The real (ε') part of relative permittivity and tan δ in the frequency range of 40 Hz–1 MHz of porous $BaTiO_3$ and $Ba(Ti_{0.96}Sn_xZr_{0.04-x})O_3$ (x = 0.02−0.04) ceramics at room temperature is shown in **Figures 7** and **8**, respectively. It can be seen that the value of dielectric constant is higher at lower frequencies and decreases with increase in frequency. The decrease of dielectric constant with increasing frequency means that the response of the permanent dipoles decreases as the frequency increases and the contribution of the charge carriers (ions) toward the dielectric constant decreases [41, 42].

Sample	Theoretical density (d_{xrd}) (g/cm^3)	Experimental density (d_{exp}) (g/cm^3)	Relative density (%)	% porosity	Grain size (nm)
$BaTiO_3$	6.02	5.639	93.6	6.3	144.53
$Ba(Ti_{0.96}Sn_{0.02}Zr_{0.02})O_3$	6.17	5.382	87.2	12.8	199.65
$Ba(Ti_{0.96}Sn_{0.03}Zr_{0.01})O_3$	6.19	5.418	87.5	12.4	84.54
$Ba(Ti_{0.96}Sn_{0.04})O_3$	6.18	5.502	89.0	10.9	89.28

Table 2. Physical properties of $BaTiO_3$ and $Ba(Ti_{0.96}Sn_xZr_{0.04-x})O_3$ (x = 0.02–0.04) ceramics.

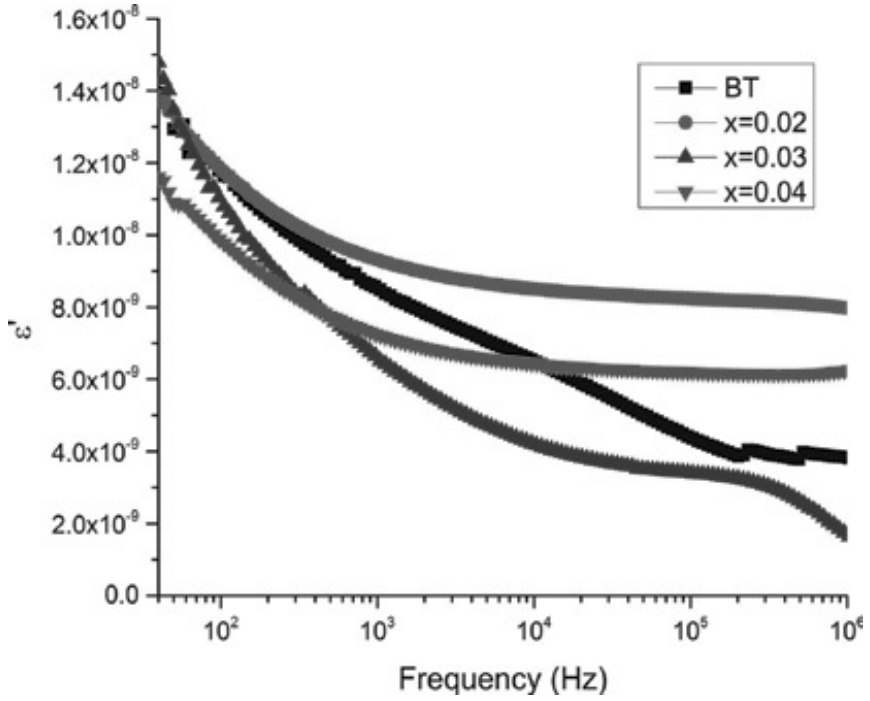

Figure 7. Variation of the real part of relative permittivity (ε′) of nanocrystalline $BaTiO_3$ and $Ba(Ti_{0.96}Sn_xZr_{0.04-x})O_3$ (x = 0.02–0.04) at 30°C.

The ε′ for BT has a value of only 1550 at room temperature which is lower than that of the sample prepared by conventional solid-state reaction route [43, 44]. The observed lower value is as a result of the smaller grain size of the ceramics [45, 46]. With the reduction of crystallite size that corresponds to the width of the domain wall, pinning would be formulated inside the grains and the domain wall motion would be inhibited. The domain wall mobility reduction leads to the decrease of the switching rate, hence lowering the dielectric constant. The presence of tin in the material also decreases the dielectric constant of Ba $(Ti_{0.96}Sn_{0.04})O_3$ [47, 48]. The observed lowering of the dielectric constant for $Ba(Ti_{0.96}Sn_{0.04})O_3$ could be considered as a combined effect of the presence of Sn and the nanocrystalline nature of the grains.

The increase of dielectric constant from 1563 to 1671 (**Table 3**) in porous $Ba(Ti_{0.96}Sn_{0.02}Zr_{0.02})O_3$ and $Ba(Ti_{0.96}Sn_{0.03}Zr_{0.01})O_3$, respectively, may be as a result of decrease of grain size and porosity of the sample. The frequency-independent behavior of è for $Ba(Ti_{0.96}Sn_{0.02}Zr_{0.02})O_3$ and $Ba(Ti_{0.96}Sn_{0.04})O_3$ beyond 1000 Hz indicates the reduction of the contribution of the charge carriers toward the dielectric permittivity ε′ and tends to a static value at all temperatures as a result of absence of space charge effects [49]. Further, the ε′ exhibits high value which reflects the effect of space charge polarization and/or conducting ion motion. The best sample is Ba $(Ti_{0.96}Sn_{0.03}Zr_{0.01})$ O_3 because it exhibited high real dielectric relative permittivity of 1671, loss of 1.63 and low porosity of 12.4% among the doped samples. This shows that the sample Ba $(Ti_{0.96}Sn_{0.03}Zr_{0.01})O_3$ can be used for MLCCs and energy storage application.

http://dx.doi.org/10.5772/intechopen.75500

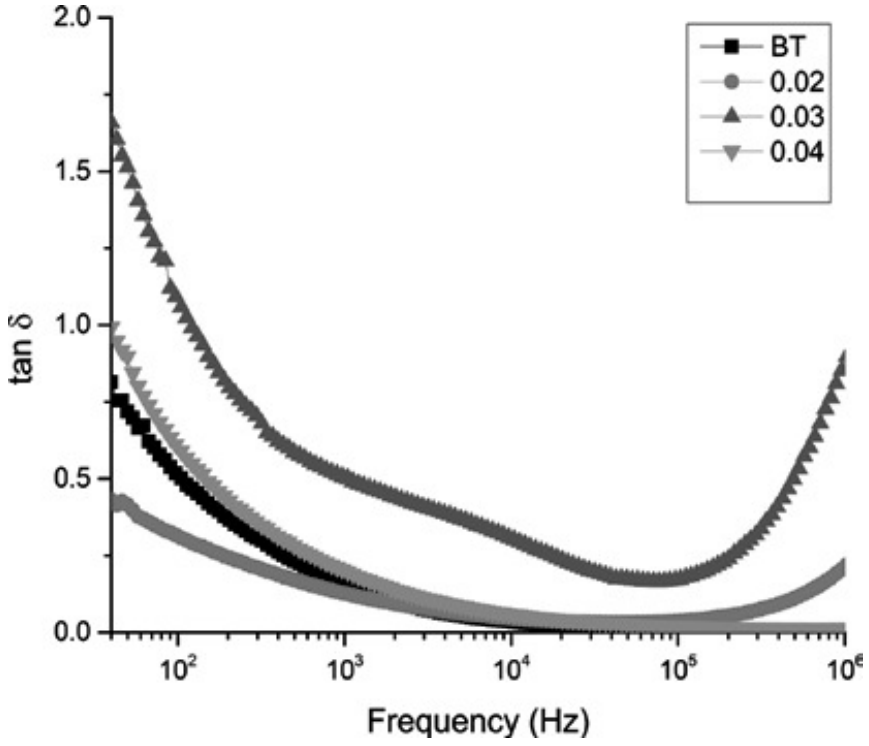

Figure 8. Frequency dependence of dielectric loss (tan δ) of $BaTiO_3$ and $Ba(Ti_{0.96}Sn_xZr_{0.04-x})O_3$ (x = 0.02–0.04) at 30°C.

Samples	E_c (kV/cm)	P_r (μC/cm^2)	P_s (μC/cm^2)
BT	0.592	0.295	1.934
BTSZ1	1.766	0.576	1.411
BTSZ2	2.930	3.117	4.680
BTSZ3	2.894	3.726	5.120

Table 3. Ferroelectric properties of the samples at room temperature.

The variation of tan δ with frequency is shown in **Figure 8**. Similar to the behavior of ε′ with frequency, the dielectric loss exponentially decreases with decreasing frequency to almost zero for porous $BaTiO_3$ and $Ba(Ti_{0.96}Sn_{0.04})O_3$.but rises beyond 10^5 Hz for $Ba(Ti_{0.96}Sn_{0.02}Zr_{0.02})O_3$ and $Ba(Ti_{0.96}Sn_{0.03}Zr_{0.01})O_3$, respectively. In the lower frequency region, a decrease in the value of tan δ is observed which is due to the dominance of space charge polarization and interface effects at lower frequencies. However, for porous $BaTiO_3$ and $Ba(Ti_{0.96}Sn_{0.04})O_3$ at a frequency of 10^4Hz, frequency-independent behavior of these parameters is observed. The values of tan δ of $BaTiO_3$ and $Ba(Ti_{0.96}Sn_xZr_{0.04-x})O_3$ (x = 0.02−0.04) are shown in **Table 3**. The decrease of tan δ in $BaTiO_3$ from 0.8 to 0.43 and from 1.6 at x = 0.03 to 0.43 at x = 0.02 clearly indicates that loss tangent shows a decreasing tendency with increase of zirconium content in agreement with literatures [50]. The dielectric losses were a combined result of electrical conduction and orientational polarization of the matter [51].

3.2.2. Variation of dielectric constant and tangent loss with temperature

The variation of dielectric constant and tangent loss as a function of temperature for porous $BaTiO_3$ and $Ba(Ti_{0.96}Sn_xZr_{0.04-x})O_3$ (x = 0.02−0.04) ceramics measured from room temperature to 150°C at the frequency of 100 Hz is shown in **Figures 9** and **10**, respectively. From **Figure 9**, it is clear that the maximum dielectric constant of porous $BaTiO_3$ and $Ba(Ti_{0.96}Sn_xZr_{0.04-x})O_3$ (x = 0.02−0.04) is at room temperature and decreases with increase in temperature, though less than that reported in CuO-modified $Ba(Ti_{0.96}Sn_xZr_{0.04-x})O_3$ (x = 0.02−0.04) ceramics synthesized using solid-state reaction [44] except for porous BT where the dielectric constant was observed to decrease from 30 to 70°C and then increased sharply at 90°C. Thereafter, it falls to the lowest level at 110°C, thus indicating a phase transition. For porous $Ba(Ti_{0.96}Sn_xZr_{0.04-x})O_3$ (x = 0.02−0.04) ceramics, the phase transition seems to be shifted toward lower room temperature with increase in doping concentration as reported by other workers [52]. The shifting of transition temperature (*Tc*) to a lower value can be explained by the larger radius of Sn^{4+} (0.69 Å) and Zr^{+4} (0.72 Å), compared to Ti^{4+} (0.605 Å). Uchino et al. have suggested that with decreasing grain size, T_c was shifted downward toward room temperature, eventually tending toward 0 K at some critical particle size [53].

In **Figure 10**, the dielectric loss of $Ba(Ti_{0.96}Sn_xZr_{0.04-x})O_3$ (x = 0.02−0.04) beyond 70°C becomes almost independent and later merges at higher temperature, except for $BaTiO_3$ which rapidly increases with increase in temperature beyond 90°C. This sharp increase in dielectric loss in the

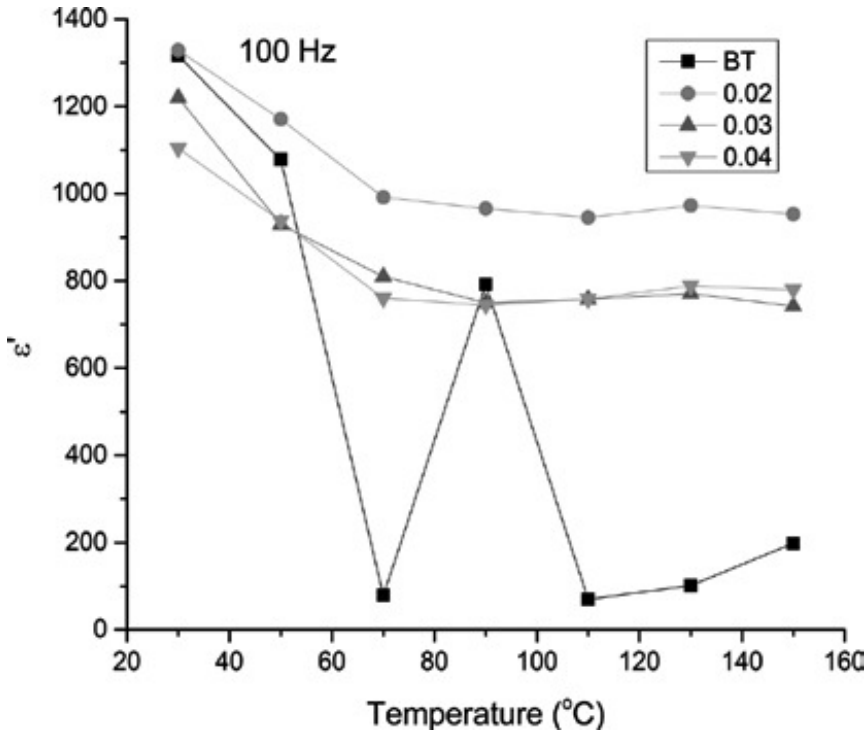

Figure 9. Temperature dependence of dielectric constant of nanocrystalline $BaTiO_3$ and $Ba(Ti_{0.96}Sn_xZr_{0.04-x})$ O_3(x = 0.02–0.04) ceramics measured at 100 kHz.

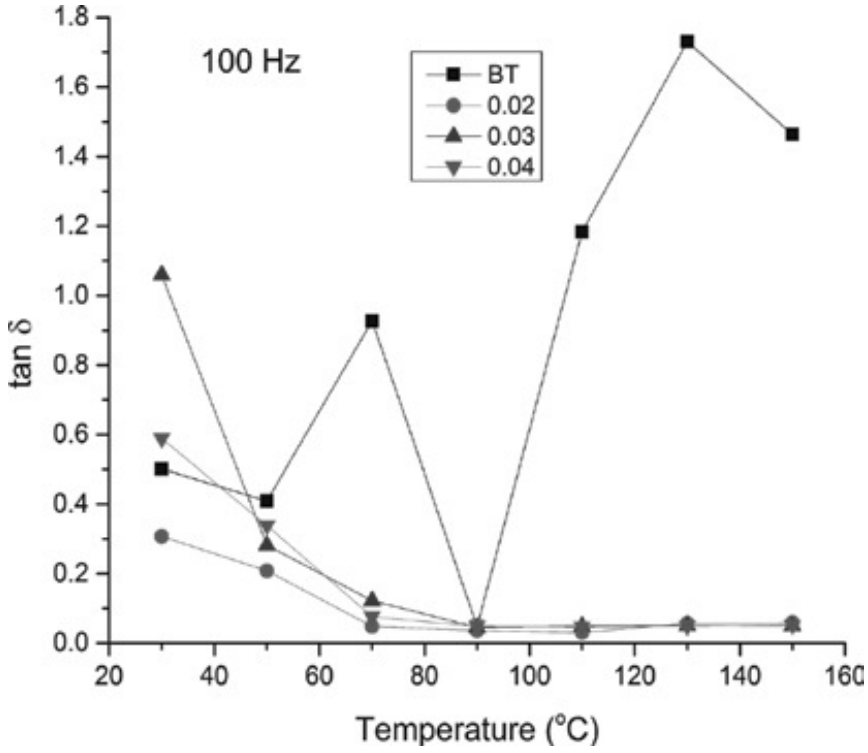

Figure 10. Temperature dependence of dielectric loss of nanocrystalline $BaTiO_3$ and $Ba(Ti_{0.96}Sn_xZr_{0.04-x})O_3$ (x = 0.02–0.04) ceramics measured at 100 kHz.

high temperature region in $BaTiO_3$ may be attributed to the increased mobility of charge carriers arising from defects or vacancies in the sample [54]. In porous $BaTiO_3$ sample, the minimum in the dielectric loss is coincident with the maximum of dielectric anomaly. Therefore, we conclude that porous $BaTiO_3$ sample undergoes a structural phase transition. The loss tangent of porous $Ba(Ti_{0.96}Sn_xZr_{0.04-x})O_3$ (x = 0.02−0.04) ceramics decreases with increasing Zr content due to the chemical stability of Zr^{4+} compared to that of Ti [55].

3.3. Ferroelectric properties

The polarization versus electric field (P-E) hysteresis loops of $BaTiO_3$ and $Ba(Ti_{0.96}Sn_xZr_{0.04-x})O_3$ (x = 0.02−0.04) ceramics measured at room temperature and 1 kHz with different Sn concentrations are shown in **Figure 11**. The results are presented in **Table 3**. The polarization hysteresis loop is not fully saturated which may be due to leakage current. The *P-E* loops become larger and broader as the Sn content (x) increases which show the ferroelectricity of the $Ba(Ti_{0.96}Sn_xZr_{0.04-x})O_3$ (x = 0.02−0.04). The increase in Remnant polarization is due to the increase in the dielectric property and decrease of the porosity of the sample with an increase in Sn doping [56]. The performance parameter of BT is very close to that of the reported values (P_s of 2.0 μC/cm^2, E_c of 5 kV/cm) for the ceramic sample [57] and lower than the one obtained by the same synthesis route (P_r of 2.0μC/cm^2, and coercive field (E_c) of 1060 V/cm) [35]. The decrease of E_c for 2.8 to 2.6 kV/cm for $Ba(Ti_{0.96}Sn_{0.03}Zr_{0.01})O_3$ to $Ba(Ti_{0.96}Sn_{0.04})O_3$ may be

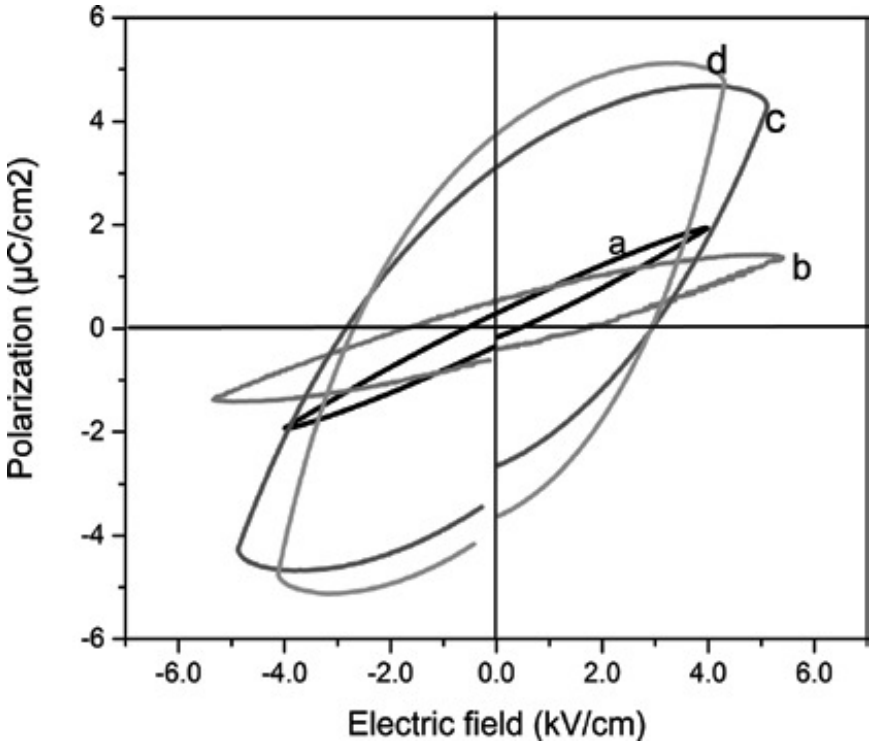

Figure 11. P-E hysteresis loop of nanocrystalline ceramics synthesized at 1190°C: (a) BT, (b) 0.02, (c) 0.03, and (d) 0.04.

attributed to the reduction in grain size and indicates that $Ba(Ti_{0.96}Sn_{0.04})O_3$ may be useful for switching applications. $BaTiO_3$ samples have cubic phase and ferroelectric tetragonal phase ($Ba(Ti_{0.96}Sn_{0.02}Zr_{0.02})O_3$, $Ba(Ti_{0.96}Sn_{0.03}Zr_{0.01})O_3$ and $Ba(Ti_{0.96}Sn_{0.04})O_3$) as evident from XRD result. Polarization reversal of a ferroelectric domain is much easier inside a larger grain the comparison to that in a smaller grain [58]. Oxygen vacancies may affect domain wall motion by a screening of the polarization charge. A formation ion of mechanical barriers against the domain walls by oxygen vacancies, that is, domain wall pinning, might also stabilize the domain configuration.

3.4. Complex impedance

Figure 12 shows the variation of the real (Z') and imaginary (Z'') part of impedance (inset) with frequency from 200 to 400°C. It is observed that the magnitude of Z' decreases with increase in frequency at different temperatures which is an indication of an increase in dc conductivity. The coincidence of Z' and Z'' values at higher frequencies at all temperatures indicates a possible release of space charge [59] and a consequent lowering of the barrier properties of the material [60]. Further, at low frequencies, the Z' values decrease with rise in temperature, that is, they show negative temperature coefficient of resistance (NTCR) behavior similar to semiconductors [61].

http://dx.doi.org/10.5772/intechopen.75500

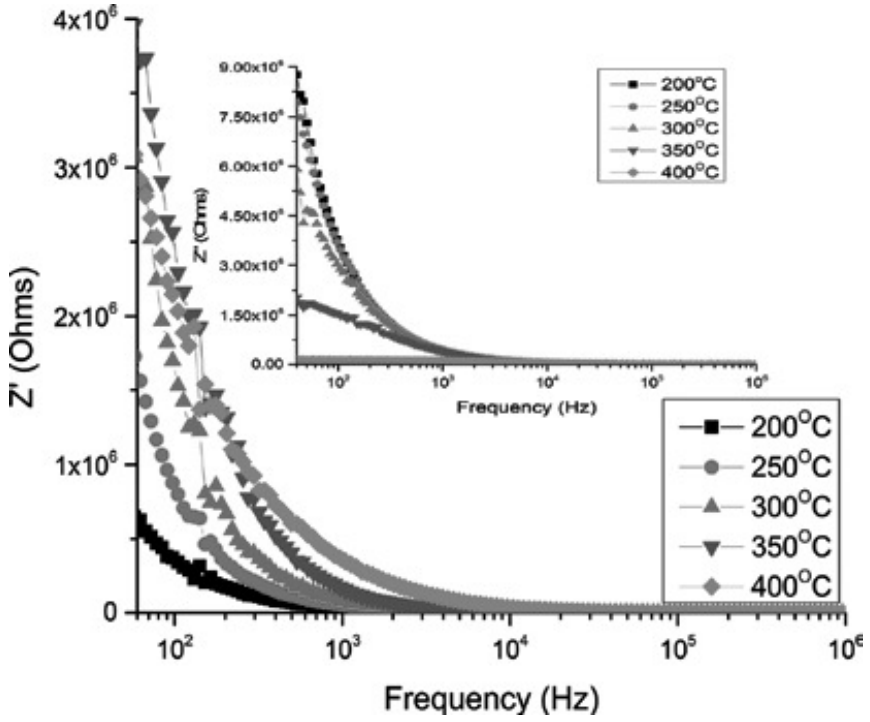

Figure 12. Frequency dependences of real (Z′) and imaginary (Z″) part of impedance (inset) of nanocrystalline Ba $(Ti_{0.96}Sn_{0.02}Zr_{0.02})O_3$ sample at 200–400°C.

Figure 13 shows the complex impedance plots (Z^*) or Cole-Cole plots, that is, plotting imaginary part Z'' against the real part Z' of complex impedance $Z^* = Z' + jZ''$ of BTSZ ceramic, performed at 200, 250, 300 and 350°C over a wide frequency range (40 Hz to 1 MHz). From **Figure 13**, it is observed that with the increase in temperature, the slope of the lines decreases and the curve moves toward real (Z') axis indicating an increase in conductivity of the sample.

At temperature 400°C, two semicircles are formed (**Figure 14**) representing resistance for grain (R_g) and grain boundary (R_{gb}) effect in the material having centers lying below the real axis confirming the presence of the non-Debye type of relaxation phenomenon in the materials [62]. Hence, grain and grain boundary effects in **Figure 14** could be separated at these temperatures. The high-frequency semicircle corresponds to a bulk contribution, and the low-frequency semicircle corresponds to the grain boundary effect [63]. The value of bulk resistance (R_g) in the high-frequency range and grain boundary resistance (R_{gb}) in the low-frequency range obtained from the intercepts of the semicircular arcs formed at 400°C on the real axis (Z') is 44.08 and 148.4 kΩ, respectively (**Figure 14**). The observed data were modeled on an equivalent circuit having a series combination of two parallel resistor-capacitor elements (inset of **Figure 14**) [64, 65]. The real (Z') and imaginary (Z'') parts of total impedance of the equivalent circuit are defined as:

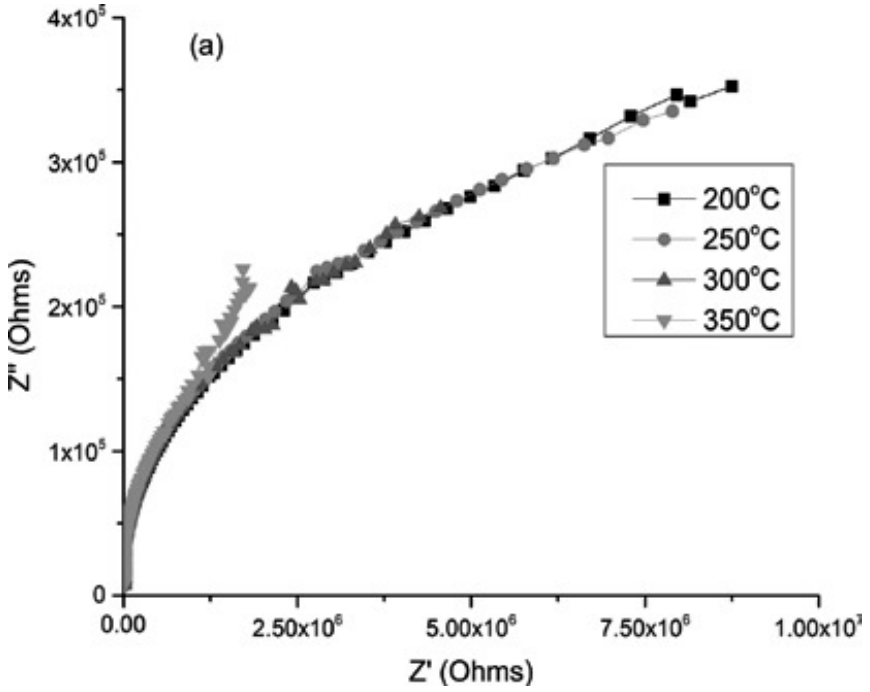

Figure 13. Plot of Z' versus Z'' (Nyquist or Cole-Cole plots) for nanocrystalline $Ba(Ti_{0.96}Sn_{0.02}Zr_{0.02})O_3$ ceramic data taken over a wide frequency range of 40 Hz to 1 MHz at 200–350°C.

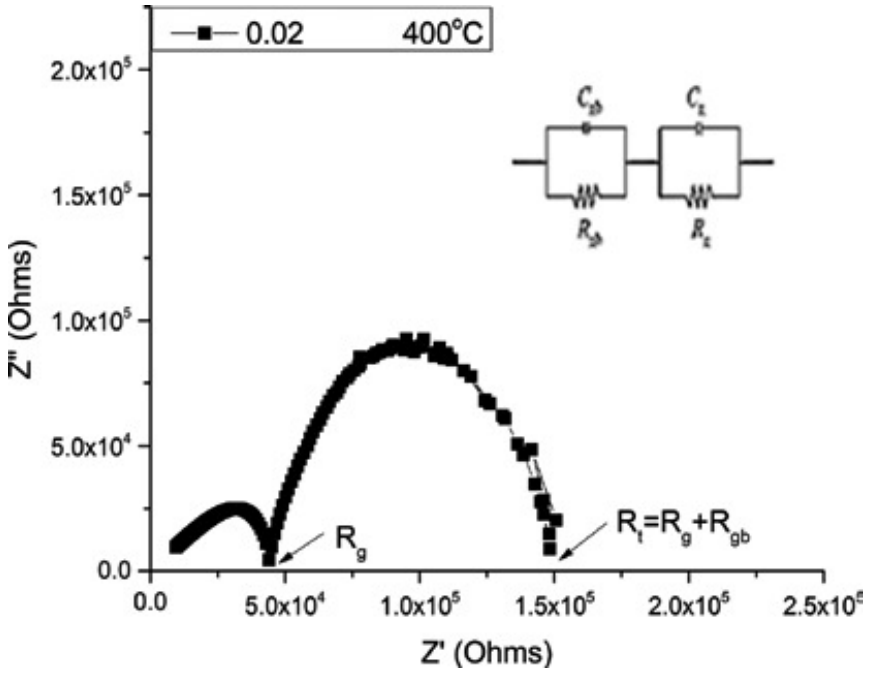

Figure 14. Plot of Z' versus Z'' (Nyquist or Cole-Cole plots) for nanocrystalline $Ba(Ti_{0.96}Sn_{0.02}Zr_{0.02})O_3$ ceramic data taken over a wide frequency range of 40 Hz to 1 MHz at 400°C.

$$Z' = \frac{R_g}{1 + \left(\omega R_g C_g\right)^2} + \frac{R_{gb}}{1 + \left(\omega R_{gb} C_{gb}\right)^2} \tag{5}$$

$$Z'' = R_g \left[\frac{\omega R_g C_g}{1 + \left(\omega R_g C_g\right)^2}\right] + R_{gb} \left[\frac{\omega R_{gb} C_{gb}}{1 + \left(\omega R_{gb} C_{gb}\right)^2}\right] \tag{6}$$

where R_g and Cg are the grain resistance and grain capacitance, R_{gb} and C_{gb} are the grain boundary resistance and grain boundary capacitance at the interfacial regions, respectively, and ω is the angular frequency. The semicircles in the impedance spectrum have a characteristic peak occurring at a unique relaxation frequency ($\omega_{max} = 2\pi f_{max}$) which can be expressed as $\omega_{max}RC = \omega_{max}\ \tau = 1$, where "$f$ max" is the frequency at the maximum of semicircle. Therefore,

$$f_{max} = \frac{1}{2\pi\tau} = \frac{1}{2\pi RC} \tag{7}$$

where τ is the relaxation time. The respective capacitances (C_b and C_{gb}) due to the grain and grain boundary effects can be calculated using Eq. 7. The values of R_g, R_{gb}, C_g and C_{gb} obtained from Cole-Cole plots at 400°C are 44.17 kΩ, 148.43 kΩ, 3.23×10^{-10} Farad and 1.71×10^{-8} Farad, respectively. The corresponding relaxation times due to both the bulk and grain boundary effect (τ_g and τ_{gb}) have been calculated using Eq. 7 to be 1.42×10^{-5} s and 2.55×10^{-3} s, respectively.

Moreover, the results showed a higher value of R_{gb} as compared to R_g as a result of a lower concentration of oxygen vacancies and trapped electrons in grain boundaries. This is due to the loss of oxygen during high temperature sintering process which again greatly influenced the conduction and dielectric relaxation behavior of the material. High temperature sintering leads to the formation of oxygen vacancies as $2O_o^x \rightarrow O_2(g) + 2V\ddot{o} + 4e^-$. Nevertheless, when the temperature is slowly cooled to room temperature in air, a reoxidation process occurs as $2V\ddot{o} + O_o^x + 4e^- \rightarrow O_2(g)$ and leads to the formation an insulating grain boundary and highly conductive oxygen-deficient grains [66].

4. Conclusion

In this study, porous $BaTiO_3$ and $Ba(Ti_{0.96}Sn_xZr_{0.04-x})O_3$ (x = 0.02−0.04) ceramics with nanocrystalline structure were obtained by mechanochemical synthesis method. The effects of the porosity of the ceramics on their microstructural and dielectric properties were investigated. It was found that porosity of the ceramics could be tailored by varying the dopant content. With increase of Sn content, porosity decreased from 12.8 to 10.9%. X-ray analysis confirms the cubic and tetragonal structure at room temperature for pristine and Zr and Sn codoped barium titanate, respectively. FESEM images indicated that the particles possess a porous structure. The temperature dependence dielectric study revealed a normal ferroelectric behavior in the material. Room temperature dielectric constant increased with Sn and Zr content, while

dielectric loss decreased. Electrical parameters such as the real part of impedance (Z'), the imaginary part of impedance (Z'') as a function of both frequency and temperature have been studied through impedance spectroscopy. Nyquists plots of $Ba(Ti_{0.96}Sn_{0.02}Zr_{0.02})O_3$ ceramic show both bulk and grain boundary effects at 400°C which indicates the NTCR behavior of the sample. Therefore, $Ba(Ti_{0.96}Sn_{0.02}Zr_{0.02})O_3$ ceramic is considered as a promising low-cost material for thermistor applications. The electrical relaxation process occurring in the material has been found to be temperature dependent.

Author details

Umaru Ahmadu[1]*, Alhassan Muazu[2] and Sadiq Umar[3]

*Address all correspondence to: u.ahmadu@yahoo.com

1 Department of Physics, Federal University of Technology, Minna, Nigeria

2 Department of Physics, Federal College of Education (T), Bichi, Kano, Nigeria

3 Department of Physics, Ahmadu Bello University, Zaria, Nigeria

References

[1] Stojanovic BD, Mastelaro VR, Paiva Santos CO, Varela JA. Structure study of donor doped barium titanate prepared from citrate solutions. Science of Sintering. 2004;**36**:179-188

[2] Haertling GH. Ferroelectric ceramics: History and technology. Journal of American Ceramic Society. 1999;**82**(4):797-818

[3] Uchino K. Ferroelectric Devices. New York: Marcel Dekker; 2000

[4] Jaffe B, Cook WR, Jaffe H. Piezoelectric Ceramics. London: Academic Press Limited; 1971

[5] Shi T, Xie L, Gu L, Zhu J. Why Sn doping significantly enhances the dielectric properties of $Ba(Ti_{1-x}Sn_x)O_3$. Scientific Reports. 2015;**5**:8606. DOI: 10.1038/srep08606

[6] Lu SG, Xu ZK, Chen H. Tunability and relaxor properties of ferroelectric barium stannate titanate ceramics. Applied Physics Letters. 2004;**85**(22):5319-5321

[7] Wei X, Yao X. Preparation, structure and dielectric property of barium stannate titanate ceramics. Material and Science Engineering, B. 2007;**137**:184

[8] Kumar SU, Reddy VR, Bag P, Rawat R, Gupta SM, Gupta A. Electro-caloric effect in lead-free Sn doped $BaTiO_3$ ceramics at room temperature and low applied fields. Applied Physics Letters. 2014;**105**:112907. DOI: 10.1063/1.4896044

[9] Xie L, Li YL, Yu R, Cheng ZY, Wei XY, Yao X, Jia CL, Urban K, Bokov AA, Ye Z-G, Zhu J. Static and dynamic polar nanoregions in relaxor ferroelectric $Ba(Ti_{1-x}Sn_x)O_3$ system at high temperature. Physical Review B. 2012;**85, 014118**

[10] Zhi Y, Guo R, Bhalla AS. Dielectric behavior of $Ba(Ti_{1-x}Zr_x)O_3$ single crystals. Journal of Applied Physics. 2000;**88**(1):410. DOI: 10.1063/1.373674

[11] Stojanovic BD, Foschini CR, Pavlovic VB, Pablovic VM, Pejovic V, Varela JA. Barium titanate screen-printed thick films. Ceramics International. 2002;**28**(3):293-298. DOI: 10.1016/S0272-8842 (01)00093-1

[12] Zhao J, Li L, Wang Y, Gui Z. DC bias properties of $Ba(Ti_{1-x}Zr_x)O_3$ ceramics. Material Science and Engineering, B. 2003;**99**(1–2):207-210

[13] Jiang JZ, Poulsen FW, Mørup S. Structure and thermal stability of nanostructured iron-doped zirconia prepared by high-energy ball milling. Journal of Materials Research. 1999; **14**:1343-1352

[14] Martin L, Chu Y, Ramesh R. Advances in the growth and characterization of magnetic, ferroelectric, and multiferroic oxide thin films. Materials Science and Engineering R. 2010; **68**:89-133. DOI: 10.1016/j.mser.2010.03.001

[15] Gong X, She WH, Hoppenjans EE, Wing ZN, Geyer RG, Halloran JW, Chappell WJ. Tailored and anisotropic dielectric constants through porosity in ceramic components. IEEE Transactions on Microwave Theory and Techniques. 2005;**53**:3638-3647

[16] Fang TT, Hsieh HL, Shiau F. Effects of pore morphology and grain size on the dielectric properties and tetragonal–cubic phase transition of high-purity barium titanate. Journal of the American Ceramic Society. 1993;**76**(5):1205-1211. DOI: 10.1111/j.1151-2916.1993. tb03742.x

[17] Wing ZN, Wang B, Halloran JW. Permittivity of Porous Titanate Dielectrics. Journal of the American Ceramic Society. 2006;**89**:3696. https://doi.org/10.1111/j.15512916.2006.01323.x

[18] Dang ZM, Zhou T, Yao SH, Yuan JK, Zha JW, Song HT, Li JY, Chen Q, Yang WT, Bai J. Advanced calcium copper titanate/polyimide functional hybrid films with high dielectric permittivity. Journal of Advanced Materials. 2009;**21**(20):2077-2082. DOI: 10.1002/ adma.200803427

[19] Jhaa AK, Prasad K. Ferroelectric $BaTiO_3$ nanoparticles; biosynthesis and characterization. Colloids and Surfaces, B: Biointerfaces. 2010;**75**:330-334

[20] Larsen G, Lotero E, Nabity M, Petkovic LM, Shobe DS. Surfactant-assisted synthesis of mesoporous zirconia powders with high surface areas. Journal of Catalysis. 1996;**164**:246-248. DOI: 10.1006/jcat.1996.0379

[21] Corma A. From microporous to mesoporous molecular sieve materials and their use in catalysis. Chemical Reviews. 1997;**97**(6):2373-2420. DOI: 10.1021/cr960406n

[22] Victor F, Stone J, Davis R. Synthesis, characterization, and photocatalytic activity of titania and niobia mesoporous molecular sieves. Chemistry of Materials. 1998;**10**(5):1468-1474. DOI: 10.1021/cm980050r

[23] German RM. Sintering Theory and Practice. New York: Wiley; 1996

[24] Wang S, Ding J, Shi Y, Chen YJ. High coercivity in mechanically alloyed $BaFe_{10}A_{l2}O_{19}$. Journal of Magnetism and Magnetic Materials. 2000;**219**:206-212

[25] Macdonald JR. Impedance Spectroscopy—Emphasizing Solid Materials and Systems. New York: Wiley-Interscience; 1987

[26] Ahmadu U, Tomas Ŝ, Jonah SA, Musa AO, Rabiu N. Equivalent circuit models and analysis of impedance spectra of solid electrolyte $Na_{0.25}Li_{0.75}Zr_2(PO_4)_3$. Advanced Materials Letters. 2013;**4**(3):185-195

[27] Jacob R, Harikrishnan Nair G, Isac J. Impedance spectroscopy and dielectric studies of nanocrystalline iron doped barium strontium titanate ceramics. Processing and Application of Ceramics. 2015;**9**(2):73-79

[28] Gomez-Yanez C, Benitez C, Ramirez HB. Mechanical activation of the synthesis reaction of $BaTiO_3$ from a mixture of $BaCO_3$ and TiO_2 powders. Ceramics International. 2000;**26**: 271-277

[29] Berbenni V, Marini A, Bruni G. Effect of mechanical milling on solid state formation of $BaTiO_3$ from $BaCO_3$-TiO_2 (rutile) mixtures. Thermochimica Acta. 2001;**374**:151-158

[30] Brzozovski E, Castro MA. Lowering the synthesis temperature of high-purity $BaTiO_3$ powders by modifications in the processing conditions. Thermochimica Acta. 2003;**398**: 123-129

[31] Ding JS, Suzuki T, McCormic PG. Ultra fine particles prepared by mechanical/thermal processing. Journal of the American Ceramic Society. 1996;**79**:2956-2958

[32] Giri AK. Nanocrystalline materials prepared through crystallization due to instability in amorphous materials after grinding. Advanced Materials. 1997;**9**:163-166

[33] Buttner RH, Maslen EN. Structural parameters and electron difference density in $BaTiO_3$. Acta Crystallographica Section B. 1992;**B48**:764-769

[34] Burtr L, Jianping Z. Preparation, structure evolution and dielectric properties of barium titanate thin fim and powder by an aqueous sol-gel process. Thin Solid Films. 2001;**388**:107

[35] Lazarevi ZZ, Vijatovi M, Doh MZ, Rom NZ, Rom MJ, Paunovi N, Stojanovi BD. The characterization of the barium titanate ceramic powders prepared by the Pechini type reaction route and mechanically assisted synthesis. Journal of the European Ceramic Society. 2010;**30**:623-628

[36] Pengrong R, Zicheng L, Qian W, Biaolin P, Shanming K, Huiqing F, Gaoyang Z. Large nonlinear dielectric behavior in $BaTi_{1-x}Sn_xO_3$. Scientific Reports. 2017;**7**:6693. DOI: 10.1038/s41598-017-07192-x

[37] Al-Naboulsia T, Boulos M, Tenailleau C, Dufour P, Zakhour M, Sophie G-F. Elaboration and characterization of barium titanate powders obtained by the mechanical activation of barium nitrate and titanate oxide, and electrical properties of the ceramics sintered by SPS. Journal of Ceramic Processing Research. 2016;**17**(8):870-875. ISSN 1229-9162

[38] Hou YD, Chang LM, Zhu MK, Song XM, Yan H. Effect of $Li_2CO_3Li_2CO_3$ addition on the dielectric and piezoelectric responses in the low-temperature sintered 0.5PZN–0.5PZT systems. Journal of Applied Physics;**102**:2007, 084507. DOI: 10.1063/1.2800264

[39] Srikanth KS, Singh VP, Vaish R. Enhanced pyroelectric figure of merits of porous $BaSn_{0.05}Ti_{0.95}O_3$ ceramics. Journal of the European Ceramic Society. 2017;**37**(13):3943-3950. DOI: 10.1016/j.jeurceramsoc.2017.05.015

[40] Yang KY, You WJ, Krishnamurthy A. Effect of porosity on electrical stability of hydrocarbon polymeric low-k dielectric. IEEE Transactions on Electron Devices. 2005;**52**(10):2333-2336

[41] Graca M, Valente MA, Ferreira da Silva MG. Electrical properties of lithium niobium silicate glasses. Journal of Non-Crystalline Solids. 2003;**325**(1–3):267-274

[42] Bergo P, Pontuschka WM, Prison JM. Dielectric properties of P_2O_5-$N_{i2}O$-L_{i2} glasses containing WO_3, CoO or Fe_2O_3. Solid State Communicaions. 2007;**141**(10):545-547

[43] Shao SF, Zhang JL, Zhang Z, Zheng P, Zhao ML, Li JC, Wang CL. High piezoelectric properties and domain configuration in $BaTiO_3$ ceramics obtained through the solid-state reaction route. Journal of Physics and Dielectric: Applied Physics. 2008;**41**(12):125408

[44] Tan YQ, Zhang JL, Wang CL. High piezoelectric properties and good temperature stabilities of CuO-modified $Ba(Ti_{0.96}Sn_xZr_{0.04-x})O_3$ ceramics. Journal of Advanced Dielectrics. 2013;**3**(2):1350014

[45] Wu K, Schulze W. Aging of the weak-field dielectric response in fine- and coarse-grain ceramic $BaTiO_3$. Journal of the American Ceramic Society. 1992;**75**(12):3390-3395. DOI: 10.1111/j.1151-2916.1992.tb04439.x

[46] Frey MH, Payne DA. Grain-size effect on structure and phase transformations for barium titanate. Physics Review. 1996;**B54**:3158-3168

[47] Isupov VA. Some p5roblems of diffuse ferroelectric phase transitions. Ferroelectrics. 1989; **90**(1):113-118. DOI: 10.1080/00150198908211278

[48] Nath AK, Medhi N. Density variation and piezoelectric properties of $Ba(Ti_{1-x}Sn_x)O_3$ ceramics prepared from nanocrystalline powders. Bulletin of Materials Science. 2012; **35**(5):847-852

[49] Ahmadu U, Tomas Ŝ, Musa AO, Isah KU. Electrical and dielectric characterization of $Na_{0.5}Li_{0.5}Zr_2(PO_4)_3$. Open Journal of Physical Chemistry. 2011;**1**:94-103

[50] Zheng P, Zhang JL, Shao SF, Tan YQ, Wang CL. Piezoelectric properties and stabilities of CuO-modified $Ba(Ti,Zr)O_3$ ceramics. Applied Physics Letters. 2008;**94**:032902. DOI: 10.1063/1.3072347

[51] Gattu S, Dasari KS, Kocharlakota VR. Structural and dielectric properties of Sn doped barium magnesuim zirconium titanate perovskite ceramics. World Journal of Condensed Matter Physics. 2015;**5**:346-352. DOI: 10.4236/wjcmp.2015.54035

[52] Alkathya MS, Joseph A, Raju KCJ. Dielectric properties of Zr substituted barium strontium titanate. Materials Today: Proceedings. 2016;**3**:2321-2328

[53] Uchino K, Sadanaga E, Hirose T. Dependence of the crystal structure on particle size in barium titanate. Journal of the American Ceramic Society. 1989;**72**(8):1555-1558. DOI: 10.1111/j.1151-2916.1989.tb07706.x

[54] Ganguly P, Jha AK. Journal of Alloys and Compound. 2010;**495**:7-12

[55] Sagar R, Hudge P, Madolappa S, Kumbharkhane AC, Raibagkar RL. Electrical properties and microwave dielectric behaviour of holmium substituted barium zirconium titanate ceramics. Journal of Alloys and Compound. 2012;**537**:197

[56] Yadav KL, Sharma P. Indian Journal of Engineering & Materials Sciences. 2008;**15**:61

[57] Deshpande SB, Potdar HS, Patil MM, Deshpande VV, Khollam YB. Dielectric properties of $BaTiO_3$ ceramics prepared from powders with bimodal distribution. Journal of Industrial and Engineering Chemistry. 2006;**12**(4):584-588

[58] Leu CC, Chen CY, Chien CH. Domain structure study of $SrBi_2Ta_2O_9$ ferroelectric thin films by scanning capacitance microscopy. Applied Physics Letters. 2003;**82**(20):3493-3495. DOI: 10.1063/1.1576308

[59] Plocharski J, Wieczoreck W. PEO based composite solid electrolyte containing NASICON. Solid State Ionics. 1988;**979**:28-30

[60] Kumar A, Singh BP, Choudhary RNP, Thakur AK. Characterization of electrical properties of Pb-modified $BaSnO_3$ using impedance spectroscopy. Materials Chemistry and Physics. 2006;**99**(1):150-159

[61] Sarangi S, Badapanda T, Behera B, Anwar S. Frequency and temperature dependence dielectric behavior of barium zirconate titanate nanocrystalline powder obtained by mechanochemical synthesis. Journal of Materials Science: Materials in Electronics. 2013; **24**:4033-4042. DOI: 10.1007/s10854-013-1358-0

[62] Ranjan R, Kumar N, Behera B, Choudhary RNP. Investigations of Impedance and Electric Modulus Properties of Pb1-xS mx$(Zr_{0.45}Ti_{0.55})$1x/4O_3ceramics. Advanced Materials Letters. 2014;**5**(3):138-142

[63] Ganguly P, Jha AK, Deori KL. Complex impedance studies of tungsten–bronze structured $Ba_5SmTi_3Nb_7O_{30}$ ferroelectric ceramics. Solid State Communications. 2008;**146**(11-12):472-477

[64] Hirose N, West AR. Impedance spectroscopy of undoped $BaTiO_3$ ceramics. Journal of the American Ceramic Society. 1996;**79**:1633-1641. DOI: 10.1111/j.1151-2916.1996.tb08775.x

[65] Dutta A, Bharti C, Sinha TP. AC conductivity and dielectric relaxation in CaMg1/3Nb2/3O_3. Materials Research Bulletin. 2008;**43**(5):1246-1254

[66] Morrison FD, Sinclair DC, West AR. Characterization of lanthanum doped barium titanate ceramics using impedance spectroscopy. Journal of the American Ceramic Society. 2001;**84**:531-538